Determination of hair cell metabolic state in isolated cochlear preparations by two-photon microscopy

LeAnn M. Tiede
Sonia M. Rocha-Sanchez
Richard Hallworth
Creighton University
Department of Biomedical Sciences
Omaha, Nebraska 68178

Michael G. Nichols
Creighton University
Department of Biomedical Sciences
    and Department of Physics
Omaha, Nebraska 68178

Kirk Beisel
Creighton University
Department of Biomedical Sciences
Omaha, Nebraska 68178

Abstract. Currently there is no accepted method to measure the metabolic status of the organ of Corti. Since metabolism and mitochondrial dysfunction are expected to play a role in many different hearing disorders, here for the first time we employ two-photon metabolic imaging to assess the metabolic status of the cochlea. When excited with ultrashort pulses of 740-nm light, both inner and outer hair cells in isolated murine cochlear preparations exhibited intrinsic fluorescence. This fluorescence is characterized and shown to be consistent with a mixture of oxidized flavoproteins (Fp) and reduced nicotinamide adenine dinucleotide (NADH). The location of the fluorescence within hair cells is also consistent with the different mitochondrial distributions in these cell types. Treatments with cyanide and mitochondrial uncouplers show that hair cells are metabolically active. Both NADH and Fp in inner hair cells gradually become completely oxidized within 50 min from the time of death of the animal. Outer hair cells show similar trends but are found to have greater variability. We show that it is possible to use two-photon metabolic imaging to assess metabolism in the mouse organ of Corti. © 2007 Society of Photo-Optical Instrumentation Engineers. [DOI: 10.1117/1.2714777]

Keywords: cochlea; nicotinamide adenine dinucleotide; flavoprotein; metabolic imaging; inner hair cells; outer hair cells.

Paper 06149SSR received Jun. 5, 2006; revised manuscript received Sep. 29, 2006; accepted for publication Oct. 20, 2006; published online Mar. 20, 2007.

1 Introduction

It has been long recognized that mitochondria play a critical role in living cells by generating ATP, maintaining cellular redox potential, and detoxifying reactive oxygen species (ROS) and xenobiotics.[1] More recently, the roles of mitochondria in generating apoptotic signals and the permeability transition in acute necrotic injury have been described. Because of the high energy demands of neurons and the generation of high levels of ROS, the nervous system is particularly vulnerable to mitochondrial dysfunction. Mitochondria in neurons play significant roles in intracellular Ca^{2+} homeostasis by sequestering[2,3] Ca^{2+} and regulating synaptic transmission.[4] In general, mitochondrial dysfunction can lead to a multisystem disorder that includes the central nervous system, peripheral nervous system, endocrine, cardiac, ocular, auditory, gastrointestinal, renal, myoskeletal, dermal, and hematological abnormalities. Progressive late onset mitochondriopathies are thought to be associated with age-related diseases and are based on diminished mitochondrial function due to progressive DNA damage (i.e., heteroplasmy) and deterioration of energy production.[5]

In the auditory system, mitochondrial defects are associated with initial deterioration and loss of high-frequency sensitivity in presbycusis, noise-induced hearing loss, and many inherited forms of hearing impairment and loss.[6,7] The role of mitochondrial dysfunction in hearing loss (HL) is supported by syndromic and nonsyndromic deafness associated with mitochondrial mutations[8] and the direct effects of ototoxic drugs such as aminoglycosides and cisplatin.[8,9] Furthermore, defects in mitochondria are associated with the effect of noise-, age- and ROS-related insults.[10,11] Noise, ototoxic, and ischemia-induced HL are also thought to be cumulative processes that are suggested to be, in part, mediated by ROS.[12,13] More recently, mice carrying a mutation either in the proofreading-deficient version of the mitochondrial DNA (mtDNA) polymerase α (POLA) or the γ subunit (POLG) accumulate mtDNA mutations and display features of accelerated aging and HL (Refs. 14 and 15). Mitochondrial changes, such as swelling and long-term degeneration, are observed in HL. Further alterations associated with mitochondrial metabolic defects are documented by immunohistochemical studies of mitochondrial enzymes. Despite this wealth of information, little to no direct evidence for metabolic changes in cochlear mitochondria is available.

Current imaging techniques are available to document the metabolic status of mitochondria in living cells. The reduced form of the nicotinamide adenine dinucleotide coenzyme (NADH) and the oxidized forms of flavoproteins (Fp) have been widely used as intrinsic fluorescent probes of mitochondrial respiration since development of this approach by Chance and Baltscheffsky,[16] Chance et al.,[17] and Chance and

---

Address all correspondence to: Michael G. Nichols, Department of Physics, 2500 California Plaza, Creighton University, Omaha, Nebraska 68178. Tel: 402-280-2159; Fax: 402-280-2140; E-mail: mnichols@creighton.edu

Shoener.[18] NADH fluorescence has been widely used in monitoring the metabolic status of cornea, brain, muscle, and other tissue.[19–25] Fp fluorescence can be used as a complementary technique showing the relative oxidized state rather than the reduced state shown by NADH fluorescence.[26,27] The use of this paired technique has also been used to characterize cardiac myocytes.[28,29]

Two-photon excitation of these intrinsic fluorophores is advantageous because the amount of energy required to cause cellular damage increases exponentially with the wavelength of the light, resulting in reduced phototoxicity.[30,31] Further, the simultaneous absorption of two near-IR photons confines both the fluorescence and the subsequent photobleaching to the focal plane.[32] NADH can be imaged with submicrometer resolution using multiphoton microscopy.[33–40] Two-photon excitation in the range of 710 to 780 nm causes NADH to emit a broad blue fluorescence peaking near 460 nm. Flavoproteins can be similarly imaged using a broad range of excitation wavelengths (700 to greater than 900 nm) with a fluorescence emission peak near 530 nm. Two-photon redox ratiometric fluorimetry of NADH and cellular flavoproteins has been performed in cardiac myocytes.[31] More recently, two-photon-excited NADH imaging has been employed to study astrocytes and neurons in living brain slices.[35,37] In addition, two-photon NADH imaging with one-photon Fp imaging was used to study the pyruvate response in pancreatic islets.[38]

In previous studies of cultured rat basophilic leukemia cells,[39] we showed that the NADH fluorescence is primarily localized to mitochondria, and that this fluorescence shows appropriate responses to mitochondrial inhibitors and unancouplers. However, we were unable to measure two-photon-excited Fp fluorescence in this cultured cell line. We also studied NADH photobleaching during multiphoton microscopy to optimize metabolic imaging techniques.[40] Here, we build on this work to develop functional two-photon imaging of excited NADH and Fp to study the metabolic state of neurosensory epithelium, hair cells, in the cochlea. We employed an isolated murine cochlea preparation similar to that used in many prior studies of cochlear physiology. This technique enabled us, for the first time, to do direct cell-by-cell metabolic characterization and determine general metabolic parameters for different cell types within the organ of Corti from the same images. Further development of this technique can be employed to study metabolic function in hearing disorders using a wide variety of animal models, including the spontaneous and genetically engineered mutant mouse lines.

2 Materials and Methods

2.1 Materials

Our materials included a cochlea preparation medium: L-15 medium (Gibco, Grand Island, New York) with 10-mM Hepes, pH 7.3; imaging medium: 135-mM NaCl, 5-mM KCl, 1-mM $MgCl_2 \cdot 6H_2O$, 1.8-mM $CaCl_2 \cdot 2H_2O$, 20-mM Hepes, 5-mM glucose, 0.5% (by volume) bovine serum albumin, pH 7.3; sodium cyanide (NaCN), cyanide-p-trifluoromethoxy-phenyl hydrazone (FCCP); NADH solution: 1-mM NADH in phosphate buffered saline, pH 7.2; and FMN solution: 10 μM flavin mononucleotide (FMN) in phosphate buffered saline, pH 7.2. Unless otherwise stated,
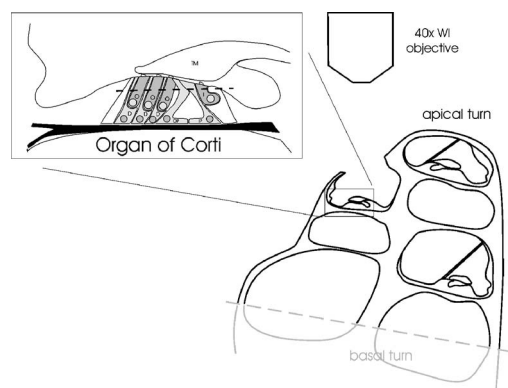
Fig. 1 Cross-sectional diagram of the prepared cochlea with a microscope objective shown above the viewing area. The objective looks down on the organ of Corti, and images are taken of the outer hair cells (O), outer and inner pillar cells (OP, IP), and inner hair cells (I), through the tectorial membrane (TM), which is located above these cells, as shown in the inset.

all chemicals were obtained from Sigma-Aldrich, St. Louis, Missouri.

2.2 Mouse Dissection

Mice (CF-1, Charles River Laboratories, Boston, Massachusetts) were euthanized with carbon dioxide. We immediately removed the cochlea from the skull and placed it into cold L-15 medium. Excess bone and tissue were trimmed away. Removal of the bone from the basal turn enabled the cochlea to sit level for mounting in a secure stage. A window was opened in the bone covering the apical turn of the organ of Corti, exposing the last third of the turn, as shown in Fig. 1. The preparation was inserted into a silastic tubing collar, which further stabilized it for imaging at room temperature. Animal care and handling was in accordance with an Institutional Animal Care and Use Committee (IACUC) approved protocol.

2.3 Two-Photon Microscopy

The organ of Corti was exposed to intense near-IR illumination at 740 nm by two-photon laser-scanning microscopy. Femtosecond pulses of near-IR illumination from a tunable Chameleon XR laser (Coherent Inc., Santa Clara, California) were scanned across the sample by an LSM510 META NLO laser scanning microscope with a 40×, 0.8-numerical aperture (NA) water immersion objective (Carl Zeiss Inc., Thornwood, New York). The region of interest was located below the tectorial membrane, as shown in the inset of Fig. 1, where the focal plane is indicated with a dashed line. An average laser power of 55.0 ± 0.5 mW (measured at the tissue surface) was used to excite intrinsic fluorophores. This fluorescence originated approximately 30 μm below the tissue surface. The fluorescence emission was separated into two detection channels using a 500-nm long-pass dichroic (500 DCXR, Chroma Technology, Brattleboro, Vermont) and detected by photomultiplier tubes without descanning. Blue fluorescence originating primarily from NADH was isolated using a custom-made bandpass filter (HQ460/80, Chroma Technology, Brattleboro, Vermont). Green fluorescence containing a mixture of NADH and Fp emission was isolated using an

HQ540/60 bandpass filter (Chroma Technology, Brattleboro, Vermont). These channels were later unmixed for quantitative assessment of NADH and Fp fluorescence. Eight scans were acquired and averaged to produce a single image. The spatial resolution was determined to be approximately 1 μm radially (in the image plane) by 3.5 μm axially (depth of the imaging plane), by imaging 60-nm fluorescent polystyrene spheres (Bangs Laboratories Inc., Fishers, Indiana) suspended in agarose gel (data not shown). To obtain emission spectra from individual pixels, the fluorescence was diverted to a diffraction grating and detected in 22 wavelength bands centered from 382 to 618 nm using the META detector of the LSM510 microscope. The spectral resolution was approximately 10.8 nm. No attempt was made to measure or correct for any nonuniform spectral response of the META detector.

2.4 Metabolic Treatments

To assess the metabolic state of the organ of Corti cells, intrinsic fluorescence images were taken of the organ of Corti bathed in imaging media. Then the preparation was incubated at room temperature in imaging media with 10-μM NaCN for 5 min before a second image was taken. The preparation was then rinsed with imaging media and allowed 10 min to recover. The addition of 10-μM FCCP was followed by a 5-min incubation period at room temperature before the image acquisition.

2.4.1 Spectral image analysis

Individual cells were selected as regions of interest (ROIs) in each of the spectral images (ALICE, Hayden Image Processing Group, Boulder, Colorado). The total fluorescence intensity for each cell at each wavelength was determined by summing pixel values within the ROIs for each image. The average wavelength-dependent background intensity was determined from regions of the image devoid of cells. This value was then multiplied by the number of pixels in a cellular ROI to determine the background for the region, and subtracted from the total fluorescence. The result was used as the wavelength-dependent fluorescence intensity of the individual cell. The average and standard error of the fluorescence intensities for the cells in each image were plotted as a function of the wavelength of the image (Origin, OriginLab, North Hampton, Massachusetts) to determine the average cellular fluorescence emission spectrum.

2.5 Linear Unmixing

The fluorescence emission of NADH is broad, completely overlapping the emission spectrum of FMN, as is evident in Fig. 2. While it is relatively easy to choose appropriate bandpass filters to isolate NADH emission from FMN, it is impossible to isolate FMN emission from NADH. Therefore, to determine the amount of NADH fluorescence present in the 510- to 570-nm channel, and the amount of FMN fluorescence in the 420- to 500-nm channel, we measured the fluorescence intensity present in both channels when pure solutions of either NADH or FMN were two-photon excited at 740 nm. This measurement revealed that $85\pm1\%$ of the NADH signal present in the 420- to 500-nm channel was also present in the 510- to 570-nm channel, while only $1.47\pm0.01\%$ of the FMN signal in the 510- to 570-nm chan-
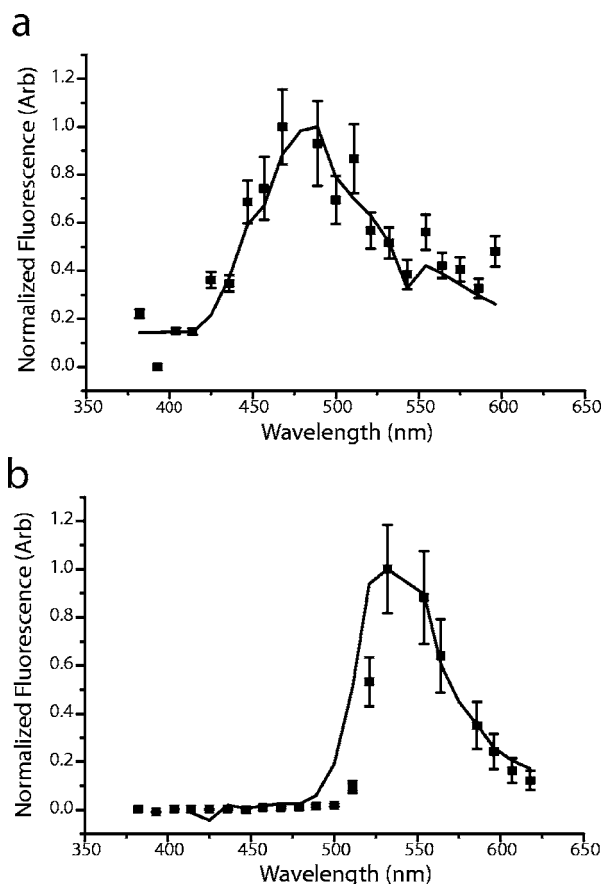
Fig. 2 Spectrum of organ of Corti cells compared with solutions. The normalized fluorescence signal is shown as a function of wavelength. (a) The spectrum of freshly prepared cells (points) is overlaid with the spectrum of a 1-mM NADH solution (line) obtained from the META detector. The points and error bars represent the mean and standard deviation of the fluorescence intensity from 32 individual cells. (b) The spectrum of isolated hair cells after digestion (points) is overlaid with a 10-μM FMN spectrum (line) obtained on the same detector. The points and error bars represent the mean and standard deviation of the fluorescence intensity from 11 individual cells.

nel was present in the 420- to 500-nm channel. Given the relatively good agreement between the fluorescence emission spectra of organ of Corti cells and free NADH and FMN in solution (Fig. 2) and the broad detection bandpass, the separated NADH and Fp channels could be obtained from the mixed channels by a linear unmixing:

$$\text{NADH} = \gamma(C_1 - 0.0147C_2), \qquad (1)$$

$$\text{Fp} = \gamma(C_2 - 0.853C_1), \qquad (2)$$

where C_1 and C_2 are the actual pixel values detected in the blue (420- to 500-nm) and green (510- to 570-nm) channels, respectively, and γ is an arbitrary scale factor that sets the display contrast. Pixel-by-pixel linear unmixing was performed for all of the images shown using ImageJ (Ref. 41).

2.6 Metabolic Image Analysis

Individual cells from images of untreated, NaCN-treated, and FCCP-treated preparations were selected in the manner de-

scribed for the spectral images. Inner hair cells (IHCs) and outer hair cells (OHCs) were identified by their well-known spatial arrangement in the organ of Corti. Background subtraction was found to be unnecessary after examining the pixel histograms, and the average pixel brightness of the cells was used for the rest of the analysis. Linear unmixing was necessary to separate the Fp and NADH fluorescence. The cellular fluorescence for IHCs and OHCs was averaged for each preparation and each treatment. The NaCN treatment produced the greatest reduction of cellular NADH and Fp, while the FCCP treatment produced the greatest concentration of the oxidized forms of these molecules. To form a relative redox scale, the percent reduction of NADH was determined by

$$\%R = \left(\frac{F_n - F_{n,u}}{F_{n,i} - F_{n,u}} \right) \times 100, \tag{3}$$

where F_n is the average cellular fluorescence obtained from the NADH channel; $F_{n,i}$ is the average cellular NADH fluorescence from the inhibited, NaCN-treated image; and $F_{n,u}$ is the average NADH fluorescence from the uncoupled, FCCP-treated preparation. All of these values correspond to the unmixed NADH fluorescence, as already described. Using the unmixed Fp fluorescence data the amount of oxidized Fp was given by

$$\%O = \left(\frac{F_{Fp} - F_{Fp,i}}{F_{Fp,u} - F_{Fp,i}} \right) \times 100, \tag{4}$$

where again the subscript i denotes the inhibited, cyanide-treated preparation; and the subscript u denotes the uncoupled, FCCP-treated preparation. The uncertainty in the fractions was estimated using the standard error of the averages for the values obtained in each category and standard error propagation techniques.[42]

2.7 Time Course Image Analysis

To determine the stability of the organ of Corti preparation, intrinsic fluorescence images were taken at 5 min intervals following the extraction and preparation of the cochlea. NADH fluorescence and Fp fluorescence were normalized to the initial fluorescence intensity in each unmixed channel and then the average value was taken for all the OHCs at each time point.

3 Results

The spectrum from cell types in the intact preparations comprised of IHCs and OHCs, as well as their associated supporting cells, can be seen in Fig. 2(a). The line indicating the spectrum of 1-mM NADH solution shows the same characteristic shape as the spectrum from the cells. The preparation shows what may be a small Fp signal present at 550 nm, which is overwhelmed by the more intense NADH fluorescence signal. In isolated OHCs that have undergone digestion with papain, the spectrum obtained closely resembles a solution of 10-μM FMN, as shown in Fig. 2(b). There is considerable agreement between the two peaks of the spectra, though the FMN spectrum appears to be slightly broader toward the blue.
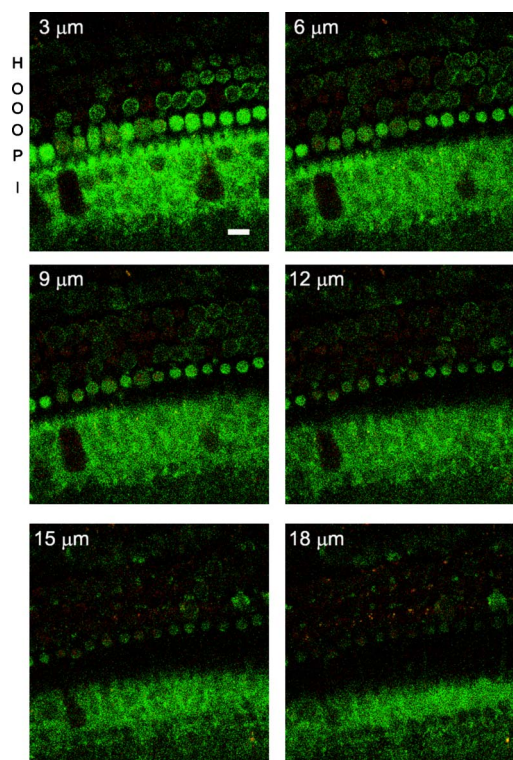
Fig. 3 Optical sections of the organ of Corti obtained 15 min after the death of the animal. The distance from the top of the OHCs is indicated on each image. A row of Hensen's cells (H), three rows of outer hair cells (O), a row of pillar cells (P), and a row of inner hair cells (I) are all visible at different points in the series. In the online version, the spectrally unmixed NADH fluorescence is represented in green, the unmixed Fp fluorescence in red, while areas of yellow indicate overlap of the two fluorescence signals. The scale bar is 10 μm. (Color online only.)

Optical sections of adjacent focal planes within the intact preparation are shown at 3.0-μm intervals in Fig. 3. The measured two-channel fluorescence images were spectrally unmixed to obtain separate NADH and Fp channels. Several rows of different cell types are apparent. The Hensen's cells are in the uppermost row as indicated by the H in Fig. 3. They exhibit a mostly even distribution of NADH fluorescence with some bright punctate regions indicative of mitochondrial clustering. The next three rows of cells, indicted by O in Fig. 3, are the OHCs. These cells have distinct rings of fluorescence that contain both NADH and Fp. The relative amount of fluorescence varies along the length of the OHC with more Fp fluorescence apparent toward the basal surface of the cells where they meet with the supporting cells underneath. The next row of cells is the pillar cells, indicated by P in Fig. 3. This row of cells is actually comprised of inner and outer pillar cells that are not separately resolved as they are pressed closely together. As the images progress deeper into the tissue, only the outer pillar cells appear to be visible. The final row of cells is comprised of IHCs, labeled I in Fig. 3. These cells are distinct because of the bright punctuate regions containing fluorescence from both Fp and NADH, corresponding to mitochondria evenly distributed throughout the cytoplasm. The nucleus appears as the dark void in IHCs. The remaining fluorescence comes from supporting cells.
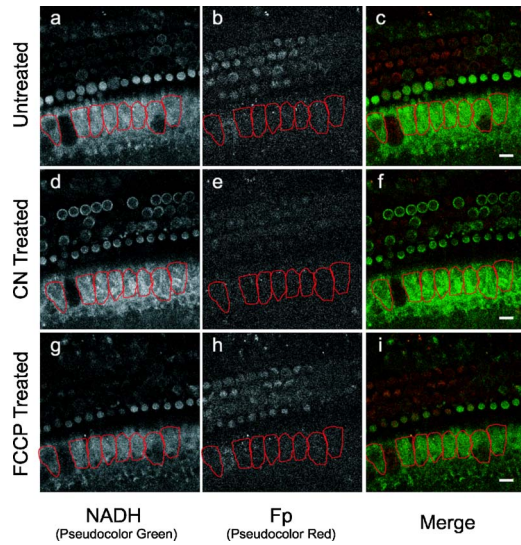
Fig. 4 Metabolic imaging of the organ of Corti at a depth of 7 μm below the top of the OHCs. The preparation (a) to (c) before the addition of any metabolic treatments to the imaging buffer, (d) to (f) after 5 min of incubation with 10-μM NaCN, and (g) to (i) after 5 min of incubation with 10-μM FCCP. Spectrally unmixed NADH fluorescence is depicted in (a), (d), and (g); unmixed Fp fluorescence in (b), (e), and (h); and a merge of NADH (pseudo-green) and Fp (pseudo-red) in (c), (f), and (i). Approximate outlines of the IHCs are drawn in red. The images were taken at 20 min (untreated), 25 min (NaCN), and 40 min (FCCP). Scale bar is 10 μm. (Color online only.)

Fig. 5 Relative metabolic state of a total of nine preparations was analyzed at seven different times. The percentage of reduced NADH (left axis) and oxidized Fp (right axis) for IHCs is shown as a function of the time between death of the animal and image acquisition for (a) IHCs and (b) OHCs. (c) NADH and Fp fluorescence normalized to the intensities of the first image and plotted as a function of time for a single preparation. Error bars represent either the standard deviation of replicated experiments or the uncertainty estimated by error propagation through Eqs. (3) and (4).

To measure the metabolic response of the cells of the organ of Corti to a mitochondrial inhibitor (NaCN) and uncoupler (FCCP), we measured fluorescence from a single focal plane approximately 7 μm below the tips of the OHCs (Fig. 4). When treated with 10-μM NaCN, OHCs and IHCs exhibited an increase in NADH fluorescence, as shown in Fig. 4(d), when compared to the preparation before treatment in Fig. 4(a). In this preparation, OHC NADH fluorescence increased to 184% of the untreated cellular NADH fluorescence, while the fluorescence of IHCs increased to only 112%. This was accompanied by a loss of Fp fluorescence that can be attributed to the decreased concentration of oxidized Fp resulting from the inhibition of oxidative phosphorylation. For OHCs, the Fp fluorescence decreased to 56% of the untreated cellular Fp fluorescence, while IHCs decreased to 89%. As expected, the trends were reversed after the preparation was treated with a 10-μM FCCP solution. When treated with FCCP, the NADH fluorescence dropped to 83 and 75% of the untreated OHC and IHC NADH fluorescence, respectively [Fig. 4(g)], and the Fp fluorescence increased to 112 and 135%, respectively [Fig. 4(h)].

The average level of reduced NADH and oxidized Fp was then calculated, using Eqs. (3) and (4), from the changes in fluorescence intensity for IHCs and OHCs. This was done for nine different preparations that were imaged at various times following the extraction of the cochlea. The results, plotted in Figs. 5(a) and 5(b), show an apparent relationship between the amount of time that the cochlea was out of the animal and the relative redox state of the hair cells. Fp oxidation increased steadily from approximately 19% at 15 min after the death of the animal, to 100% after 50 min. The IHC NADH oxidation

state followed a similar pattern, with the level of reduction decreasing from 95 to 0% within 45 min of death.

For OHCs, the results varied more dramatically, ranging from $89\pm10\%$ reduced and $21\pm19\%$ oxidized for a preparation imaged approximately 15 min after the death of the animal to $0\pm10\%$ reduced and $100\pm13\%$ oxidized after 50 min. The relationship does not appear to be linear, but is more likely to be an exponential decay. Analysis of the OHCs of a single preparation [Fig. 5(c)] showed that the ratio of reduced NADH fluorescence to oxidized Fp fluorescence decreased in

a similar manner. OHCs also began to swell as imaging time progressed with the longer time periods corresponding to a larger proportion of swollen cells.

4 Discussion

While two-photon NADH fluorescence has been imaged in brain, heart, cornea, and pancreatic tissues,[33–38] this technique had yet to be used to study metabolism in the cochlea. The spectrum of the organ of Corti cells indicates that both NADH and Fp are present in the cells in sufficient quantities for imaging. This enabled us to study the metabolism of the organ of Corti without the use of extrinsic fluorescent probes. We were also able to study the intact tissue *in toto*, with all of the different cell types, while at the same time assessing the metabolic capacity for each individual cell. The distinct histological and morphological characteristics of the organ of Corti provided a unique opportunity for metabolic imaging of whole tissue at the cellular level. There is considerable agreement between the spectral peaks of the organ of Corti cells and the NADH and FMN solutions, as shown in Fig. 2. The fluorescence spectra also show a considerable amount of overlap in the wavelengths of the NADH and Fp signals. To resolve this issue we used linear unmixing to separate the signals. This enabled us to make the first direct quantification of Fp oxidation by two-photon microscopy, rather than inferring the Fp oxidation state from the mix of NADH and Fp in the green channel, which has been used previously.

It appears that the NADH and Fp signals are present in the expected subcellular regions within the cells corresponding to the typical locations of mitochondria. This is demonstrated in Fig. 3. As described before, the distribution of the fluorescence signals in the OHC is localized in a ring nearly contiguous with the lateral wall of these cells, comprising the cellular membrane, the cortical lattice, and the subsurface cisterna. The mitochondria are located along the subsurface cisterna along the lateral wall.[43] This would produce the circular fluorescence distribution seen in the OHCs of Fig. 3. This distribution differs from the mitochondrial arrangement of IHCs. These mitochondria are dispersed throughout the cytosol, which corresponds to the punctate distribution of fluorescence as shown in Fig. 3. The pillar and Hensen's cells show a relatively even distribution of mitochondria throughout the cell, in agreement with the distribution of fluorescence in the pillar cells shown in Fig. 3. Kasischke et al.[35] showed that they were able to identify astrocytes and neurons in brain tissue based on the NADH fluorescence pattern in much the same way. This enabled us to simultaneously identify the cells of interest (IHCs or OHCs for example) as we performed metabolic imaging.

Further confirmation of the mitochondrial origin of the NADH and Fp fluorescence came when we examined the data from the metabolic treatments of cyanide and the uncoupler FCCP. After NaCN incubation, the cells should be in their most reduced state, just as if they were oxygen deprived since NaCN blocks the transfer of reducing equivalents to oxygen. NADH fluoresces when reduced, so the fluorescence should increase with the addition of cyanide. As shown in Fig. 4(d), the NADH fluorescence increased significantly after cyanide incubation, but decreased with treatment of the mitochondrial uncoupler FCCP [Fig. 4(h)]. This is expected since the uncoupler dissipates the mitochondrial pH gradient, allowing for the unregulated flow of electrons through the electron transport chain without production of ATP, rapidly converting NADH to the nonfluorescent NAD^+. The Fp fluorescence varies inversely with the NADH fluorescence, as seen in the images in Figs. 4(b), 4(e), and 4(h), as Fp fluoresces when in its oxidized state.

For all of the preparations, the sum of the relative oxidation and reduction percentages totals 100% within the uncertainty of the measurement. This is expected when the fluorescence originates from mitochondrial sources where flavin and nicotinamide cofactors are in direct equilibrium. Previous two-photon and traditional confocal metabolic imaging studies have tended to use the absolute change in intrinsic fluorescence or the ratio of the NADH and Fp fluorescence to study changes in metabolism[17,19,20,25–27,33–36] rather than quantifying the relative redox state of these molecules, as was done in this study.

The average reduction of the IHCs is $73\pm12\%$ for preparations imaged less than 40 min after the death of the animal. This is higher than we observed in cultured rat basophilic leukemia cells, which have typically been 45 and 55% reduced. This high percentage of reduced NADH and Fp indicates a large capacity for ATP production. The fact that the oxidized state predominated when images were obtained more than 40 min after the death of the animal would indicate a decreased capacity for ATP production via oxidative phosphorylation. From this study, it is unclear whether these trends result from lowered rates of regeneration of the reduced forms of NADH and Fp through glycolysis, the citric acid cycle, and beta oxidation, or from a strong upregulation of oxidative phosphorylation to produce ATP. The effect is more dramatically seen in the OHCs, as shown in Figs. 5(b) and 5(c) as the amount of reduced energy equivalents is decreasing while the amount of oxidized energy equivalents increases. It is not clear why the OHCs exhibit the loss of reduced NADH and Fp more rapidly than the IHCs.

Possible experiments that could illuminate the mechanism behind this loss of reduced NADH and Fp include varying the concentration of glucose in the media to determine if the cells are simply metabolizing glucose faster than they are able to obtain it from passive diffusion from the media. Also, potentiometric and pH-sensitive fluorescent probes may enable the assessment of ATP production resulting from oxidative phosphorylation. The temperature of the preparation may also affect the metabolism of the cells and should also be investigated. This could enable determination of the ideal working temperature of the preparation, be it physiological, room temperature, or chilled.

In developing any fluorescence imaging protocol to assess normal function of living cells it is important to minimize the adverse affects of photobleaching and photodamage.[39,40] We attempted to do this by taking relatively few images at a low sampling rate and at the lowest possible laser intensity required to get a sufficient SNR. Under these imaging conditions, we did not observe any significant NADH or Fp photobleaching. Nevertheless, we have found that photodamage during metabolic imaging can occur even when NADH photobleaching is not evident,[39] and a systematic investigation is warranted.

The Fp fluorescence images have a much lower SNR than those formed from NADH fluorescence. This is because the concentration of Fp is several orders of magnitude lower than NADH in tissue.[44] Our own experience with cultured cells has shown that the ability to detect Fp fluorescence also varies dramatically with tissue type, and, in fact, we were unable to detect Fp fluorescence in cultured rat basophilic leukemia cells.[39] Fortunately, the two-photon action cross section of Fp is more than three times that of NADH at 740 nm (Ref. 34) enabling more efficient generation of Fp fluorescence. However, the overlap in the NADH fluorescence and the Fp fluorescence also complicates the issue, making it difficult to detect the Fp fluorescence because of NADH fluorescence overlap. This was also described by Huang et al., who suggested that greater specificity for NADH and Fp could be achieved by narrowing the spectral ranges of the detection channels.[34] Unfortunately, decreasing the detection efficiency as Huang et al. suggests would further reduce the SNR of the Fp channel. Instead, we found that careful calibration of the crosstalk between the two detection channels enables the separation of the signal into its NADH and Fp components. Given the measured fluorescence emission spectrum from organ of Corti cells (Fig. 2), we expect that further improvement in measuring the weak Fp signal may be realized by extending the detection band to 650 nm.

Further experiments will determine if the amount of reduced NADH and Fp vary between species or even strains of the same animal, which would be expected from studies of dehydrogenase activity in cochleas of differing mouse strains.[45] If it can be established that there is some consistency between mammalian species, or even strains of the same species, this technique will have a very broad range of application. Studies of noise-induced hearing loss, inherited hearing loss, and presbycusis could use this technique to determine if metabolic differences exist in these hearing disorders. Combining this technique with studies of gene expression, protein function, and structural studies could help illuminate the underlying causes of some of these disorders.

References

1. J. M. Dubinsky, N. Brustovetsky, and R. LaFrance, "Protective roles of CNS mitochondria," *J. Bioenerg. Biomembr.* **36**, 299–302 (2004).
2. D. G. Nicholls, "A role for the mitochondrion in the protection of cells against calcium overload," *Prog. Brain Res.* **63**, 97–106 (1985).
3. S. Chalmers and D. G. Nicholls, "The relationship between free and total calcium concentration in the matrix of liver and brain mitochondria," *J. Biol. Chem.* **278**, 19062–19070 (2003).
4. E. Jonas, "Regulation of synaptic transmission by mitochondrial ion channels," *J. Bioenerg. Biomembr.* **36**, 357–361 (2004).
5. D. C. Wallace, "A mitochondrial paradigm of metabolic and degenerative diseases, aging and cancer: a dawn for evolutionary medicine," *Annu. Rev. Genet.* **39**, 359–407 (2005).
6. L. Van Laer, K. Cryns, R. J. Smith, and G. Van Camp, "Nonsydromic hearing loss," *Ear Hear.* **24**, 275–288 (2003).
7. M. D. Seidman and P. Vivek, "Intratympanic treatment of hearing loss with novel and traditional agents," *Otolaryngol. Clin. North Am.* **37**, 307–321 (2004).
8. N. Fischel-Ghodsiann, "Mitochondrial deafness," *Ear Hear.* **24**, 303–313 (2003).
9. T. R. Van De Water, F. Lallemend, A. A. Eshraghi, S. Ahsan, J. He, J. Guzman, M. Polak, B. Malgrange, P. P. Lefebvre, H. Staecker, and T. J. Balkany, "Caspases, the enemy within and their role in oxidative stress-induced apoptosis of inner ear sensory cells," *Otol. Neurotol.* **13**, 1953–1959 (2004).
10. A. G. Cheng, L. L. Cunningham, and E. W. Rubel, "Mechanisms of hair cell death and protection," *Cur. Opin. Otolaryngol Head Neck Surg.* **13**, 343–348 (2005).
11. J. C. Saunders, S. P. Dear, and M. E. Shneider, "The anatomical consequences of acoustic injury: a review and tutorial," *J. Acoust. Soc. Am.* **78**, 833–860 (1985).
12. K. Campbell, "Ototoxicity: understanding oxidative mechanisms," *J. Am. Acad. Audiol* **14**, 121–123 (2003).
13. J. O. Pickles, "Mutation in mitochondria as a cause of presbyacusis," *Audiol. Neuro-Otol.* **9**, 23–33 (2004).
14. A. Trifunovic, A. Wredenberg, M. Falkenberg, J. N. Johannes, A. T. Rovio, C. E. Bruder, M. Bohooly-Y, S. Gidlöf, A. Oldfors, R. Wibom, J. Törnell, H. T. Jacobs, and N. G. Larsson, "Premature ageing in mice expressing defective DNA polymerase," *Nature (London)* **429**, 417–423 (2004).
15. G. C. Kujoth, A. Hiona, T. D. Pugh, S. Someya, K. Panzer, S. E. Wohlgemuth, T. Hofer, A. Y. Seo, R. Sullivan, W. A. Jobling, J. D. Morrow, H. Van Remmen, J. M. Sedivy, T. Yamsoba, M. Tanokura, R. Weindruch, C. Leeuwenburg, and T. A. Prolla, "Mitochondrial DNA mutations, oxidative stress, and apoptosis in mammalian aging," *Science* **309**, 481–484 (2005).
16. B. Chance and H. Baltscheffsky, "Respiratory enzymes in oxidative phosphorlation VII. Binding of intramitochondrial reduced pyridine nucleotide," *J. Biol. Chem.* **233**, 736–739 (1958).
17. B. Chance, P. Cohen, F. Jobsis, and B. Schoener, "Intracellular oxidation-reduction states in vivo," *Science* **137**, 499–508 (1962).
18. B. Chance and B. Shoener, "Fluorometric studies of flavin component of the respiratory chain," in *Flavins and Flavoproteins*, E. C. Slater, Ed., pp. 510–519, Elsevier, Amsterdam (1966).
19. R. W. Estabrook, "Fluorometric measurement of reduced pyridine nucleotide in cellular and subcellular particles," *Anal. Biochem.* **4**, 231–245 (1962).
20. B. Chance, N. Oshino, T. Sugano, and A. Mayevsky, "Basic principles of tissue oxygenation determination from mitochondrial signals," in *Oxygen Transport to Tissue*, H. I. Bicher and D. F. Bruley, Eds., Plenum Press, New York (1973).
21. A. Mayevsky and B. Chance, "A new long-term method for the measurement of NADH fluorescence in intact brain with chronically implanted cannula," in *Oxygen Transport to Tissue*, H. I. Bicher and D. F. Bruley Eds., Plenum Press, New York (1973).
22. B. Chance and M. Lieberman, "Intrinsic fluorescence emission from the cornea at low temperatures: evidence of mitochondrial signals and their differing redox states in epithelial and endothelial sides," *Exp. Eye Res.* **26**, 111–117 (1978).
23. J. R. Koke and L. L. Williams, "Fluorometric measurements of changes in the NADH/NAD+ ratio in single isolated adult heart cells: effects of cyanide and 2,4-dinitrophenol," *Microbios. Lett.* **12**, 15–21 (1980).
24. A. Mayevsky and B. Chance, "Intracellular oxidation-reduction state measured *in situ* by a multichannel fiber-optic surface fluorometer," *Science* **217**, 537–540 (1982).
25. J. Eng, R. M. Lynch, and R. S. Balaban, "Nicotinamide adenine dinucleotide fluorescence spectroscopy and imaging of isolated cardiac myocytes," *Biophys. J.* **55**, 621–630 (1989).
26. R. Sholz, R. G. Thurman, J. R. Williamson, B. Chance, and T. Bucher, "Flavin and pyridine nucleotide oxidation-reduction changes in perfused rat liver," *J. Biol. Chem.* **244**, 2317–2324 (1969).

27. B. Chance, B. Schoener, R. Oshino, F. Itshak, and Y. Nakase, "Oxidation-reduction ratios studies of mitochondria in freeze-trapped samples," *J. Biol. Chem.* **254**, 4764–4711 (1979).

28. D. N. Romashko, E. Marban, and B. O'Rourke, "Subcellular metabolic transients and mitochondrial redox waves in heart cells," *Proc. Natl. Acad. Sci. U.S.A.* **95**, 1618–1623 (1998).

29. J. An, A. K. S. Camara, S. S. Rhodes, M. L. Riess, and D. F. Stowe, "Warm ischemic preconditioning improves mitochondrial redox balance during and after mild hypothermic ischemia in guinea pig isolated hearts," *Am. J. Physiol. Heart Circ. Physiol.* **288**, H2620–H2627 (2004).

30. J. M. Squirrell, D. L. Wokosin, J. G. White, and B. D. Bavister, "Long-term two-photon fluorescence imaging of mammalian embryos without compromising viability," *Nat. Biotechnol.* **17**, 763–767 (1999).

31. S. K. Mohanty, A. Rapp, S. Monajembashi, P. K. Gupta, and K. O. Greulich, "Comet assay measurements of DNA damage in cells by laser microbeams and trapping beams of wavelengths spanning a range of 308 nm to 1064 nm," *Radiat. Res.* **157**, 378–385 (2002).

32. R. M. Williams, D. W. Piston, and W. W. Webb, "Two-photon molecular excitation provided intrinsic 3-dimensional resolution for laser based microscopy and microphotochemistry," *FASEB J.* **8**, 804–813 (1994).

33. D. W. Piston, B. R. Masters, and W. W. Webb, "Three dimensionally resolved NAD(P)H cellular metabolic redox imaging of the *in situ* cornea with two-photon excitation laser scanning microscopy," *J. Microsc.* **178**, 20–27 (1995).

34. S. Huang, A. A. Heikal, and W. W. Webb, "Two-photon fluorescence spectroscopy and microscopy of NAD(P)H and flavoprotein," *Biophys. J.* **82**, 2811–2825 (2002).

35. K. A. Kasischke, H. D. Vishwasrao, P. J. Fisher, W. R. Zipfel, and W. W. Webb, "Neural activity triggers neuronal oxidative metabolism followed by astrocytic glycolysis," *Science* **305**, 99–103 (2004).

36. K. Blinova, C. Combs, P. Kellman, and R. S. Balaban, "Fluctuation analysis of NADH fluorescence signals in confocal and two-photon microscopy images of living cardiac myocytes," *J. Microsc.* **213**, 70–75 (2004).

37. H. D. Vishwasrao, A. A. Heikel, K. A. Kasischke, and W. W. Webb, "Conformational dependence of intracellular NADH on metabolic state revealed by associated fluorescence anisotropy," *J. Biol. Chem.* **280**, 25119–25126 (2005).

38. J. V. Rocheleau, W. S. Head, and D. W. Piston, "Quantitative NAD(P)H/Flavoprotein autofluorescence imaging reveals metabolic mechanisms of pancreatic islet pyruvate response," *J. Biol. Chem.* **279**, 31780–31787 (2004).

39. M. G. Nichols, E. E. Barth, and J. A. Nichols, "Reduction in DNA synthesis during two-photon microscopy of intrinsic reduced nicotinamide adenine dinucleotide fluorescence," *Photochem. Photobiol.* **81**, 259–269 (2005).

40. L. M. Tiede and M. G. Nichols, "Photobleaching of reduced nicotinamide adenine dinucleotide and the development of highly fluorescent lesions in rat basophilic leukemia cells during multiphoton microscopy," *Photochem. Photobiol.* **82**, 656–664 (2006).

41. W. S. Rasband, ImageJ, U. S. National Institutes of Health, Bethesda, Maryland, USA, http://rsb.info.nih.gov/ij/ (1997–2006).

42. P. R. Bevington and D. K. Robinson, *Data Reduction and Error Analysis for the Physical Sciences*, McGraw-Hill, New York (1992).

43. N. B. Slepecky, "Structure of the mammalian cochlea," Chap. 2 in *The Cochlea*, P. Dallos, A. N. Popper, and R. R. Fay, Eds., 45–129, Springer Verlag, New York (1996).

44. C. Y. Guezennec, F. Lienhard, F. Louisy, G. Rennault, M. H. Tusseau, and P. Portero, "*In situ* NADH laser fluorometry during muscle contraction in humans," *Eur. J. Appl. Physiol.* **63**, 36–42 (1991).

45. D. L. Ding, S. L. McFadden, J. Wang, B. H. Hu, and R. J. Salvi, "Age- and strain-related differences in dehydrogenase activity and glycogen levels in CBA and C57 mouse cochleas," *Audiol. Neuro-Otol.* **4**, 55–63 (1999).